Nature of the active silane alcoholysis catalyst in the $Ru_wCl_x(CO)_y(PMe_3)_z$ (*w*, *x*, *y*, *z* = 1 or 2) system; $Ru_2(\mu\text{-}Cl)_2Cl_2(CO)_4(PMe_3)_2$ as a new catalyst for silane alcoholysis in a polar solvent[1]

Mee-Kyung Chung, George Ferguson, Valerie Robertson, and Marcel Schlaf

Abstract: The dimeric complex $Ru_2(\mu\text{-}Cl)_2Cl_2(CO)_4(PMe_3)_2$ (**1**) forms an active silane alcoholysis complex in the polar solvent *N*,*N*-dimethylamino-acetamide (DMA). The dynamic behaviour of **1** in DMF-d_7 solution has been investigated by variable temperature (VT) ^1H NMR. The solid state structures of **1** and *cis,cis,trans*-$RuCl_2(CO)_2(PMe_3)_2$ (**3**) have been determined by single crystal X-ray diffractometry. Using ethylene glycol – triethylsilane as a model system, the catalytic activity of **1** in DMA is compared to that of a series of known silane alcoholysis catalysts, including $RhCl(PPh_3)_3$, PdX_2 (X = Cl^-, OAc^-), and *cis,cis,trans*-$[IrH_2S_2L_2]SbF_6$ (L = PPh_3, S = THF). Complex **3** is not an active silane alcoholysis catalyst in this solvent, but is active in nonpolar solvents. Its structure and spectroscopic signature is, however, different from that of a previously reported catalyst of the same composition.

Key words: silane alcoholysis, polar solvent, ruthenium catalyst.

Résumé : Dans un solvant polaire comme le *N*,*N*-diméthylacétamide (DMA), l'alcoolyse du complexe dimère $Ru_2(\mu\text{-}Cl)_2Cl_2(CO)_4(PMe_3)_2$ (**1**) donne lieu à la formation d'un complexe de silane actif. Faisant appel à la RMN du ^1H à température variable, on a étudié le comportement dynamique de **1** en solution dans le DMF-d_7. On a déterminé les structures de **1** et du *cis,cis,trans*-$RuCl_2(CO)_2(PMe_3)_2$ (**3**) à l'état solide par diffraction des rayons X par un cristal unique. Utilisant le système éthylèneglycol/triéthylsilane comme modèle, on a comparé l'activité catalytique de **1** dans le DMA avec celles d'une série de silanes connus comme catalyseurs de l'alcoolyse, y compris $RhCl(PPh_3)_3$, PdX_2 (X = Cl^-, OAc^-) et *cis,cis,trans*-$[IrH_2S_2L_2]SbF_6$ (L = PPh_3, S = THF). Dans ce solvant, ce composé **3** n'est pas un silane actif comme catalyseur de l'alcoolyse; il est toutefois actif dans les solvants non polaires. Sa structure et ses caractéristiques spectroscopiques sont toutefois différentes de celles rapportées antérieurement pour un catalyseur de même composition.

Mots clés : alcoolyse de silanes, solvant polaire, catalyseur de ruthénium.

[Traduit par la Rédaction]

Introduction

The silane alcoholysis reaction (eq. [1]) constitutes an exceptionally mild and efficient method of protecting hydroxyl functions by trialkyl or aryl-silyl groups.

[1] $$R'OH + HSiR_3 \xrightarrow{[cat.]} R'OSiR_3 + H_2(g)$$

Recieved August 20, 2000. Published on the NRC Research Press Web site at http://canjchem.nrc.ca on July, 11, 2001.

Dedicated to Professor Brian R. James on the occasion of his 65th birthday.

M.-K. Chung, G. Ferguson, V. Robertson, and M. Schlaf.[2] Department of Chemistry & Biochemistry, University of Guelph, Guelph, ON N1G 2W1, Canada.

[1]Contribution from the Guelph–Waterloo Centre for Graduate Work in Chemistry (GWC)[2].

[2]Corresponding author (telephone: (519) 824-4120 ext. 3002; fax: (519) 766-1499; e-mail: mschlaf@uoguelph.ca).

The high enthalpic driving force of the oxygen–silicon bond formation, together with the entropically favourable generation of 1 equivalent of hydrogen gas, generally results in clean and quantitative conversions. The reaction is catalyzed by a large variety of transition metal complexes (1–7). Specific examples of highly active catalysts are *cis,cis,trans*-$[IrH_2S_2L_2]SbF_6$ (L = PPh_3, S = THF) (8), *all-cis*-$RuCl_2(CO)_2(PMe_3)_2$ (9), $Co_2(CO)_8$ (10), $RhCl(PPh_3)_3$ (11–13), $IrX(CO)L_2$ (L = PR_3) (14), and $[IrCl(C_8H_{14})_2]_2$ (14). Most simply, palladium metal, generated in situ by reduction of PdX_2 (X = OAc^-, Cl^-) (15) also catalyzes the reaction. Another commercially available and metal-free catalyst system is $B(C_6F_5)_3$, recently described by Blackwell et al. (16).

Common to all these catalyst systems is that, to date, they have only been tested in nonpolar, non-coordinating organic solvents such as benzene, toluene, pentane, or methylene chloride. We are interested in applying the silane alcoholysis reaction to highly polar polyol and sugar substrates with multiple hydroxyl functions, which are insoluble in these solvents, but soluble in chemically largely inert amides such as *N*,*N*-dimethylformamide (DMF), *N*-methyl-pyrrolidin-2-one (NMP), and *N*,*N*-dimethylacetamide (DMA). In order to establish which of a selection of the known catalyst systems

 DOI: 10.1139/cjc-79-5/6-949

would tolerate the anticipated *coordinative inhibition* by the donor atoms (O, N) in these solvents, we conducted an activity evaluation of a series of catalysts in DMA using ethylene glycol and triethylsilane as a model system. In the course of this study we found that the most active homogeneous catalyst system in DMA is derived from the general composition $Ru_wCl_x(CO)_y(PMe_3)_z$ (w, x, y, z = 1 or 2), but that the structures of the active catalyst precursors are in fact $Ru_2(\mu\text{-}Cl)_2Cl_2(CO)_4(PMe_3)_2$ (**1**) or *cis,cis,trans*-$RuCl_2(CO)_2(PMe_3)_2$ (**3**) rather than *all-cis*-$RuCl_2(CO)_2(PMe_3)_2$ (**2**) as previously reported (17). The dynamic solution behaviour of dimer **1** in amide solvents, as well as the solid state structures of the complex **1** and **3** as determined by single crystal X-ray structure analysis, are reported.

Results

The conditions and reagents for the synthesis of the catalyst system $Ru_wCl_x(CO)_y(PMe_2)_z$ as published are shown in eq. [2] (17).

[2] $RuCl_3 + 2\ PMe_3 + CO(g) \xrightarrow{\text{reflux}}$ **2**

Me = 2-methoxy-ethanol

Following this procedure we obtained materials that gave inconsistent results with respect to catalytic activity and whose NMR and IR spectra in no case matched the previously reported data. Singer et al. (17) assigned the *all-cis* configuration **2** to their reaction product based on ^{1}H NMR and IR data.[3] They reported a single doublet at 1.78 ppm with $J_{H,P}$ = 12 Hz in $CDCl_3$ and two ν(CO) stretching frequencies at 2085 and 2022 cm^{-1} in Nujol. While the IR data and symmetry considerations support a *cis* position of the two CO ligands, the assignment does not match with the position of the phosphine ligands. In an *all-cis* arrangement one of the phosphines must be *trans* to the σ-donor – π-acceptor CO, while the other must be *trans* to the σ-donor – π-donor Cl^-. Two different chemical environments and chemical shifts should, therefore, result for the phosphorus and by extension carbon and proton nuclei on the two phosphine ligands, unless their shifts are fortuitously equivalent. This, however, appears to be unlikely, as the structurally very closely related complex *all-cis*-$RuCl_2(CO)_2(PMePh_2)_2$ shows two separate doublets for the methyl substituents on the phosphine ligands (18). Also the *all-cis* configuration of this complex is thermally unstable against isomerization to *cis,cis,trans*-$RuCl_2(CO)_2(PMePh_2)_2$ and only accessible through a photochemical reaction via the even more unstable *all-trans* form (Fig. 1).

The expected ^{1}H NMR of the *all-trans* form, i.e., a doublet of doublet or pseudo triplet for the methyl signals due to coupling to the two phosphorus nuclei, equally would not match the literature spectral data. These considerations together with wide variations of catalyst activity in the silane

Fig. 1. Photochemically and thermally induced stereochemical rearrangements observed for $RuCl_2(CO)_2(PMePh_2)_2$.

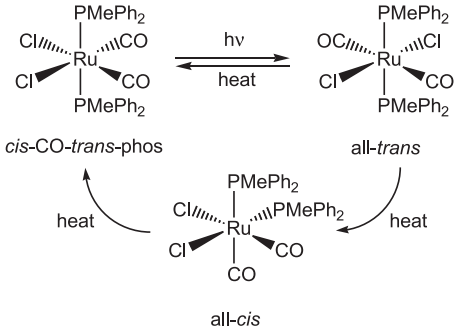

alcoholysis reactions using the material isolated by us, prompted us to reinvestigate the $Ru_wCl_x(CO)_y(PMe_3)_z$ system in more detail.

Synthesis and isolation

The reaction of eq. [2] gives an amorphous solid from which two different products of different crystal habit are obtained by fractional crystallization, first from CH_2Cl_2–Et_2O and subsequently from EtOH–H_2O. The latter solvent system is also the one used by Singer et al. (17). Single crystal X-ray diffraction analysis revealed the structure of the first product to be the dimeric complex $Ru_2(\mu\text{-}Cl)_2Cl_2(CO)_4(PMe_3)_2$ (**1**) and that of the second component to be the mononuclear complex *cis,cis,trans*-$RuCl_2(CO)_2(PMe)_2$ (**3**). The yields for both products (**1** and **3**) are between 30 and 40%, with a total yield of about 70% with respect to ruthenium. By ^{1}H and ^{31}P NMR, both compounds are present in about the same ratio in the crude product, i.e., the product identity and distribution is not an artifact of the fractional crystallization.

Structure determinations

ORTEP diagrams (19) of the structures of the dimer $Ru_2(\mu\text{-}Cl)_2Cl_2(CO)_4(PMe_3)_2$ (**1**) and that of the mononuclear complex *cis,cis,trans*-$RuCl_2(CO)_2(PMe)_2$ (**3**) are shown in Figs. 2 and 3, respectively.

Selected bond angles and distances of complexes **1** and **3** are summarized in Tables 1 and 2, respectively. The dimer **1** has a center of inversion in the plane defined by the two ruthenium centers and the bridging chloride ligands. The two Ru—Cl bond distances in this plane are, however, not equivalent, but slightly shorter (2.457 Å) for the bond *trans* to the strong π-acceptor CO and slightly longer (2.496 Å) for the bond *trans* to the phosphine, resulting in a distorted diamond shape with Cl-Ru-Cl and Ru-Cl-Ru bond angles in this plane of 83.95 and 96.04°, respectively. The Ru—Cl bond distance of the terminal chloride ligand is very close to that of an average value of 2.409 Å as reported by Orpen et al. (20) The other bond angles around ruthenium closely approach that of an idealized octahedral environment with bond lengths in the expected ranges.

All ruthenium ligand bond lengths in the mononuclear complex **3** are pairwise equivalent within the 3σ level and

[3] The original formulation in the paper by Singer et al. is: "The dérivé III (i.e., $RuCl_2(CO)_2(PMe_3)_2$) isolé possède tous ses ligands en position *cis*."

Fig. 2. Molecular structure of the dimer complex $Ru_2(\mu\text{-}Cl)_2Cl_2(CO)_4(PMe_3)_2$ (**1**) as determined by single crystal X-ray diffraction (ORTEP plot at 30% probability level).

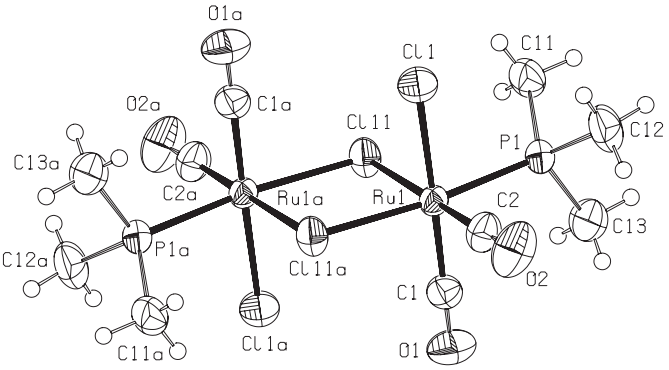

fall within the expected ranges and bond angles approach that of an idealized octahedral environment around the ruthenium center. In the solid state the two PMe_3 ligands are staggered about the P-Ru-P axis by 63.93° breaking the otherwise high symmetry of the ligand arrangement.

Spectroscopy

The spectroscopic data of **1**, **1a**, and **3** are summarized in Table 3.

Dissolving an authentic sample of X-ray grade crystals of **1** in either $CDCl_3$ or DMF-d_7 results in an ^{1}H NMR spectrum that displays two doublets for the PMe_3 ligands at the chemical shifts listed in Table 3 in relative intensities of 0.42:1, with the lower shift component as the more abundant one. Based on the high symmetry of the solid state structure of **1**, whose center of inversion would render the two phosphines chemically and magnetically equivalent, this spectral appearance immediately suggests a breakup of the dimer in solution, most likely through solvent coordination in the manner indicated in eq. [3], which retains the mutual *trans* arrangement of the π-donor chloride and π-acceptor carbonyl.

[3]

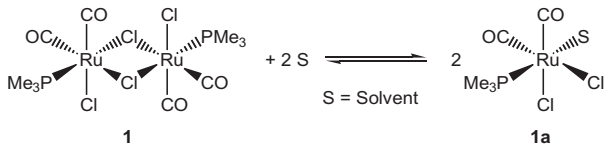

1 **1a**

The variable temperature (VT) ^{1}H NMR spectrum of the methyl signals of a sample of **1** in DMF-d_7 is shown in Fig. 4 and reveals the existence of a dynamic process in solution, which supports the above hypothesis.

The two doublets coalesce at ~100°C and reemerge as a time averaged doublet above ~120°C. In order to simplify a more quantitative analysis of this process through simulations, the VT experiment was repeated with phosphorus decoupling, which collapses the doublets into two simple coalescing singlets. Using the MEX program by Bain and Duns (21) a set of spectra were simulated that matched the these decoupled spectra over the temperature range from 65 to 124°C. From an Eyring plot of the rate constants calculated by the program vs. $1/T$ (in Kelvin) the approximate activation parameters of the process were determined to $\Delta H^{\ddagger}$ =

Fig. 3. Molecular structure of complex *cis,cis,trans*-$RuCl_2(CO)_2(PMe_3)_2$ (**3**) as determined by single crystal X-ray diffraction (ORTEP plot at 30% probability level).

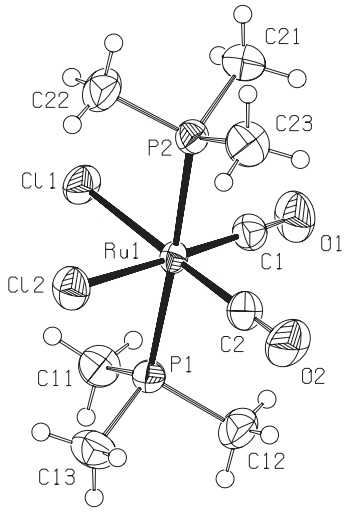

18.0 ± 0.4 kcal mol^{-1} and $\Delta S^{\ddagger}$ = –2.7 ± 0.9 cal mol^{-1} K^{-1} for the reaction of the minor to the major component ($k_{reverse}$: **1a** → **1**) and through $K_{eq} = k_f/k_r$ to $\Delta H^{\ddagger}$ = 18.4 ± 0.9 kcal mol^{-1} and $\Delta S^{\ddagger}$ = –3.0 ± 0.9 cal mol^{-1} K^{-1} for the reaction of the major to the minor component ($k_{forward}$: **1** → **1a**). Within the experimentally achievable error ranges the activation parameters are the same for the forward and the reverse reaction, which reflects an equilibrium constant K_{eq} close to unity. K_{eq} ranges from 0.45 to 0.49 in the temperature range used and was determined from the integral ratios of the ^{31}P decoupled signals at low temperatures and extrapolated for the higher temperatures, where beginning coalescence makes a reliable integration impossible.

Further support for the reaction of eq. [3] comes from the ^{13}C and ^{1}H NMR spectra of the same sample at ambient temperature. In addition to the 1:1:1 triplet for the carbonyl carbon of free DMF-d_7 at 162.7 ppm, a second small 1:1:1 triplet ($J_{C,D}$ = 30 Hz) is observed at 169.2 ppm, which we assign to the coordinated DMF-d_7 in complex **1a**. This ^{13}C signal is matched by a very small singlet at 8.45 ppm in ^{1}H NMR, which disappears with the beginning coalescence of the methyl signals and which we assign to the aldehyde proton of coordinated DMF-d_6. The signal reversibly reappears upon cooling to ambient temperature.

An unambiguous assignment of the larger and smaller sets of peaks to **1** and **1a**, respectively follows from the ^{13}C NMR signals of the carbonyl ligands. In the dimer **1** the two carbonyl ligands are chemically and magnetically inequivalent and should give rise to two doublets due to coupling to the phosphorus nucleus. In complex **1a** both carbonyl ligands are chemically and magnetically equivalent and should, thus, result only in a single doublet. Two larger doublets of approximately equal intensity are observed at 198.12 and 192.93 ppm, the latter of which overlaps with a smaller doublet at 193.08 ppm. The larger peaks must, therefore, belong to complex **1**, bearing the two nonequivalent carbonyl ligands. By extension, the larger peaks in the ^{1}H and ^{31}P NMR spectra are assigned to the dimer **1**, which is

Table 1. Selected bond lengths (Å) and angles (°) in complex **1**.

Bond lengths (Å)		**Bond angles** (°)			
Ru(1)—C(1)	1.885(3)	C(2)-Ru(1)-C(1)	91.19(11)	C(2)-Ru(1)-Cl(11a)	94.92(8)
Ru(1)—C(2)	1.855(2)	C(2)-Ru(1)-P(1)	89.85(8)	C(1)-Ru(1)-Cl(11a)	90.70(7)
Ru(1)—P(1)	2.3018(6)	C(1)-Ru(1)-P(1)	93.21(7)	P(1)-Ru(1)-Cl(11a)	173.77(2)
Ru(1)—Cl(1)	2.4018(7)	C(2)-Ru(1)-Cl(1)	89.16(9)	Cl(1)-Ru(1)-Cl(11a)	88.30(2)
Ru(1)—Cl(11)	2.4573(6)	C(1)-Ru(1)-Cl(1)	178.97(8)	Cl(11)-Ru(1)-Cl(11a)	83.955(19)
Ru(1)—Cl(11a)	2.4967(6)	P(1)-Ru(1)-Cl(1)	87.77(2)	Ru(1)-Cl(11)-Ru(1a)	96.043(19)
Cl(11)—Ru(1a)	2.4967(6)	C(2)-Ru(1)-Cl(11)	178.45(8)		
Cl(11a)—Ru(1a)	2.4573(6)	C(1)-Ru(1)-Cl(11)	89.89(7)		
O(1)—C(1)	1.126(3)	P(1)-Ru(1)-Cl(11)	91.20(2)		
O(2)—C(2)	1.128(3)	Cl(1)-Ru(1)-Cl(11)	89.74(2)		

Table 2. Selected bond lengths (Å) and angles (°) in complex **3**.

Bond lengths (Å)		**Bond angles** (°)			
Ru(1)—Cl(1)	2.4403(9)	Cl(1)-Ru(1)-Cl(2)	91.31(4)	Cl(2)-Ru(1)-P(2)	87.55(4)
Ru(1)—Cl(2)	2.4323(6)	Cl(1)-Ru(1)-P(1)	92.23(2)	Cl(2)-Ru(1)-C(1)	178.29(11)
Ru(1)—P(1)	2.3888(11)	Cl(1)-Ru(1)-P(2)	85.64(4)	Cl(2)-Ru(1)-C(2)	88.86(10)
Ru(1)—P(2)	2.3905(9)	Cl(1)-Ru(1)-C(1)	86.97(10)	P(1)-Ru(1)-P(2)	177.17(4)
Ru(1)—C(1)	1.851(2)	Cl(1)-Ru(1)-C(2)	178.77(9)	P(1)-Ru(1)-C(1)	89.45(10)
Ru(1)—C(2)	1.861(3)	Cl(2)-Ru(1)-P(1)	90.63(4)	P(1)-Ru(1)-C(2)	88.99(9)

therefore the major component in solution at ambient temperature.

The IR spectrum of the same sample of **1** dissolved in $CDCl_3$ displays only two well defined bands at 2068 and 2010 cm^{-1}, i.e., does not show the presence of two components in solution as observed by NMR. This can be rationalized by the fact that in both complexes (**1** and **1a**) both carbonyl ligands are *trans* to the same π-donor chloride and the ν(CO) stretching frequencies are, therefore, presumably very close to or even identical with each other in both complexes.

The NMR spectra of complex **3** show no dynamic phenomena and display the expected coupling patterns for the *cis*,*cis*,*trans*-arrangement. The pseudo triplet observed for the methyl signals of **3**, also establishes that it cannot have been the compound originally isolated by Singer et al. (17), whose identity remains unknown.

Evaluation of the catalysts in DMA

The catalytic activity of the new complexes **1** and **3** was evaluated using the ethylene glycol – triethylsilane system as the model reaction (eq. [4]) and compared to a series of catalyst systems consisting of *cis*,*cis*,*trans*-$[IrH_2S_2L_2]SbF_6$ (L = PPh_3, S = THF) (8), $RhCl(PPh_3)_3$ (11–13), $Co_2(CO)_8$ (10), and PdX_2, (X = Cl^-, OAc^-) (15).

[4] $$HOCH_2CH_2OH + n\ Et_3SiH \xrightarrow[-\ n\ H_2(g)]{[cat.]} \begin{matrix} HOCH_2CH_2OSiEt_3 \\ + \\ Et_3SiOCH_2CH_2OSiEt_3 \end{matrix}$$

In all reactions ethylene glycol (2.5 mmol) in DMA (6 mL) were reacted with one or two equivalents of triethylsilane at a catalyst concentration of 3 mol% with respect to metal content. Complexes **3** and $Co_2(CO)_8$ are inactive in DMA, however, **3** is an active catalyst in THF, the solvent used by Oehmichen and Singer (9). All other tested catalysts are active in the DMA solvent and quantitative results as determined by direct quantitative GC analysis of the reaction mixtures are summarized in Table 4. The data gives a direct comparison of the relative activity of the catalyst systems in the amide solvent, total yields of silylated products, as well as their selectivity towards mono- and disilylation of the diol substrate in the presence of one or two equiv of silane, respectively. The reaction times given in Table 4 refer to the end point of the reaction as indicated by the end of hydrogen gas evolution and by the complete consumption of triethylsilane as indicated by the GC trace of the reaction mixture.

Of all the catalyst systems tested, by far the most active is the dimer **1**, which even surpasses the activity of the heterogeneous palladium systems. The true catalyst of unknown structure and composition formed from **1** and triethylsilane in DMA, therefore, does not suffer from coordinative inhibition by the solvent. This contrasts with the behaviour of complex **3**, which does suffer inhibition by the solvent to the point of being inactive in the amide solvent, and the iridium system $[IrH_2(PPh_3)(THF)_2]SbF_6$, which shows as many as 130 000 turnovers per hour in methylene chloride solvent at 25°C (8), but requires heating to 45°C to achieve acceptable reaction rates in DMA. Consistent with the latter result, Crabtree et al. (22) had previously shown that the same iridium complex suffers strong inhibition by even trace amounts of coordinating solvents when used as an olefin hydrogenation catalyst. The active catalyst resulting from $RhCl(PPh_3)_3$ also must suffer coordinative inhibition, as it has been reported to give complete conversion to silane alcoholysis products within minutes in benzene solution at 20°C and catalyst concentrations as low as 0.05 mol% (13).

The yields of monosilylated product achieved by the catalysts in DMA solvent are moderate to good, but in no case

Table 3. Summary of spectroscopic data for $Ru_2(\mu\text{-}Cl)_2Cl_2(CO)_4(PMe_3)_2$ (**1**), $RuCl_2(CO)_2(PMe_3)(O{=}C(CD_3)N(CD_3)_2$ (**1a**), and *cis,cis,trans*-$RuCl_2(CO)_2(PMe)_2$ (**3**).

	1	**1a**	**3**
^{1}H NMR			
$CDCl_3$	1.67 (d, $J_{H,P}$ = 11.6 Hz)	1.70 (d, $J_{H,P}$ = 11.6 Hz)	1.68 (t, $J_{H,P}$ = 4.0 Hz)
DMF-d_7	1.74 (d, $J_{H,P}$ = 12.0 Hz)	1.81 (d, $J_{H,P}$ = 12.0 Hz)	
^{31}P{^{1}H} NMR ($CDCl_3$)	22.83 (s)	20.74 (s)	–6.70 (s)
^{13}C{^{1}H} NMR			
$CDCl_3$	too insoluble in $CDCl_3$	too insoluble in $CDCl_3$	193.27 (t, $J_{C,P}$ = 11.4 Hz, CO)
DMF-d_7	15.73 (dd, $J_{C,P}$ = 36.9, < 2 Hz, CH_3), 198.12 (d, $J_{C,P}$ = 14.8 Hz, CO), 192.93 (d, $J_{C,P}$ = 12.6 Hz, CO)	17.70 (dd, $J_{C,P}$ = 39.1, < 2 Hz, CH_3), 169.2 (t, $J_{C,D}$ = 30.0 Hz, coordinated DMF-d_7), 193.08 (d, $J_{C,P}$ = 16.2 Hz, CO)	14.86 (t, $J_{C,P}$ = 16.6 Hz, CH_3)
IR ν(CO) ($CDCl_3$)	2068, 2010	2068, 2010	2049, 1985

Note: All NMR data is reported in ppm, IR data in cm^{-1}.

Fig. 4. VT ^{1}H NMR spectrum of **1** and **1a** in DMF-d_7.

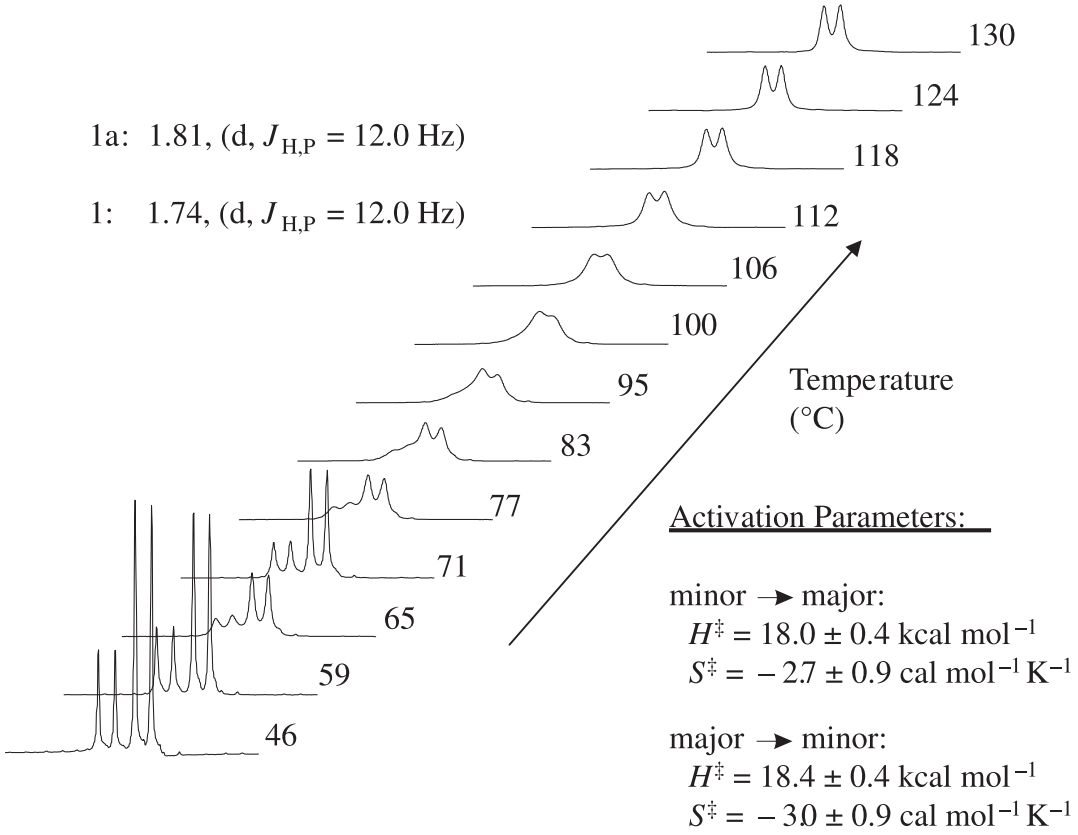

reach the near quantitative conversions to silylated products typically observed in this reaction with equimolar amounts of silane and alcohol in nonpolar solvents. Even with rigorous drying of the hygroscopic DMA solvent by distillation from barium oxide[4] under argon and subsequent storage over activated 4 Å molecular sieves, some of the silane is consumed by the reaction with adventitious water forming the silanol and siloxane side products Et_3SiOH and $Et_3SiOSiEt_3$. A control experiment in the absence of ethylene glycol also yielded Et_3SiOH and $Et_3SiOSiEt_3$ confirming the presence of water in the solvent. By GC–MS no disilane $Et_3SiSiEt_3$ could be detected in either the control or any of the actual alcoholysis reactions. Both observed side products were identified and authenticated by GC, ^{1}H NMR, and GC–MS, but not quantified. However, qualitatively the amounts of the side products formed appeared to be insufficient to explain the low yields. Even though we found no direct evidence of the solvent itself reacting with the silane,

[4] This drying agent has been suggested by Andrews (23) to be very effective for amide solvents.

Table 4. Comparison of relative catalyst activity and reaction yields (A = $Et_3SiOCH_2CH_2OH$, B = $Et_3SiOCH_2CH_2OSiEt_3$) for the silylation of ethyleneglycol with triethylsilane in DMA.

Catalyst	Et_3SiH–glycol (equiv.)	Rxn. temp. (°C)	Rxn. time (h)[a]	Yield A (%)[b]	Yield B (%)[b]	Total yield (%)[b]
$[IrH_2(PPh_3)(THF)_2]SbF_6$	1	ambient	>300	44	11	55
		45	4.2	42	11	53
	2	ambient	>300	46	40	86
		45	45	29	69	98
$Ru_2(\mu\text{-}Cl)_2Cl_2(CO)_4(PMe_3)_2$	1	ambient	<0.1	54	9	63
		0	1.1	50	8	58
	2	ambient	<0.1	58	32	90
		0	2.3	55	41	96
$RhCl(PPh_3)_3$	1	ambient	50	50	9	59
		45	12.5	44	7	51
	2	ambient	71	61	29	90
		45	14.8	39	61	100
$PdCl_2$	1	ambient	0.9	41	11	52
		0	1.7	46	19	65
	2	ambient	1.2	44	44	88
		0	4.5	22	78	100
$Pd(OAc)_2$	1	ambient	0.2	56	11	67
		0	4.75	46	6	52
	2	ambient	0.8	61	28	89
		0	4.0	61	28	S 89

Note: Reaction conditions in all cases: 2.5 mmol ethylene glycol in 6 mL of DMA, 3 mol% metal.
[a]End point of reaction indicated by the end of hydrogen gas evolution and complete consumption of Et_3SiH as confirmed by GC.
[b]By quantitative GC with respect to ethylene glycol.

i.e., there are no unaccounted peaks in the GC traces of the silylation reactions, we cannot exclude the possibility that the DMA solvent signal observed in the GC contains such reaction products that do not chromatographically separate as a result of hydrogen bond interactions within the solvent.[5] Another possible explanation is that larger amounts of silanol are actually formed in the reactions, but are not detected because of a reaction with the GC injector liner and (or) the column itself.

The selectivity to monosilylation:disilylation with one equivalent of silane ranges from 1:2.4 to 1:7.7. Interestingly, the most active catalyst **1** gives some of the best selectivity at a ratio of 1:6.2 at yields comparable to those of the other catalyst systems. As expected with two equiv of triethylsilane the selectivities increasingly favour disilylation. Good yields of disilylated products are, however, only achieved by $PdCl_2$ and the iridium system.

The temperature range investigated was limited to 0–45°C, as we were only interested in reaction conditions that could ultimately be applied to more complex and very temperature sensitive polyols and sugars. Within this range no clear trend of temperature dependency of yields and selectivities can be extracted from the data. Instead the conditions for the optimization of these two goals are unique to the catalyst used.

Equation [5] shows a possible pathway of an HCl catalyzed silane alcoholysis, which is conceivable for the chloride containing catalysts.

$$[5]\quad \begin{aligned} &L_nM\text{-}Cl + H\text{-}SiR_3 \longrightarrow L_nM\text{-}SiR_3 + HCl \\ &HCl + H\text{-}SiR_3 \longrightarrow Cl\text{-}SiR_3 + H_2(g) \\ &Cl\text{-}SiR_3 + R'OH \longrightarrow R'O\text{-}SiR_3 + HCl \\ &R' = H,\ CH_2CH_2OH \end{aligned}$$

Such a pathway may, in particular, be possible in the DMA solvent, which should be capable of stabilizing highly polar intermediates. The HCl would be generated from the chloride content of the catalysts through the reaction with triethylsilane. In order to exclude this possibility, we carried out a control reaction with concentrated aq HCl added in an amount equimolar to the metal catalysts used, i.e., 3 mol% $H_3O^+Cl^-$ with respect to ethylene glycol. The control reaction asserted that HCl catalyzed processes are irrelevant, as only very small amounts of silane hydrolysis and glycol silylation products were detected even at greatly extended reaction times compared to the metal catalyzed reactions in Table 4.

Discussion

While the selectivities and yields achieved so far are only moderate, the use of DMA as a solvent extends the utility of

[5]GC columns of various polarity did not result in further resolution of the solvent DMA peak. A GC–MS investigation of the solvent peak itself is not practical as it is entirely dominated by the solvent fragmentation pattern.

Table 5. Selected single crystal X-ray crystallography parameters for **1** and **3**.

	1	**3**
Empirical formula	$C_{10}H_{18}Cl_4O_4P_2Ru_2$	$C_8H_{18}Cl_2O_2P_2Ru$
FW	608.12	380.14
Crystal size (mm)	0.40 × 0.40 × 0.20	0.41 × 0.11 × 0.08
Crystal system	Monoclinic	Monoclinic
Space group	$P2_1/c$	$P2_1/c$
a (Å)	7.8533(6)	6.6145(6)
b (Å)	11.0683(9)	8.5160(6)
c (Å)	12.4603(8)	13.6041(18)
β (°)	100.577(7)	102.010(13)
Volume (Å^3)	1064.68(14)	749.53(13)
Unit cell data range 2Θ (°)	19.11–21.02	19.10–24.50
T (K)	294(1)	294(1)
Z	2	2
$\rho_{calcd.}$ (g cm^{-3})	1.897	1.684
X-ray source (graphite monochromator)	Mo Kα; λ = 0.71073 Å	Mo Kα; λ = 0.71073 Å
μ (cm^{-1})	2.079	1.597
Refinement	F^2	F^2
Reflections measured	2442	3404
Independent reflections	2442	3268
Observed reflections	2205	3085
Observation criterion	>2σ (*I*)	>2σ (*I*)
Intensity data range Θ (°)	2.48–27.47	2.84–27.47
R_1[a]	0.0199	0.0172
wR_2[a]	0.0529	0.0408
GoF	1.058	1.094

[a]Definitions of indices: $R_1 = \Sigma(F_o - F_c)/\Sigma(F_o)$; $wR_2 = [\Sigma[w(F_o^2 - F_o^2)^2]/\Sigma[w(F_0^2)^2]]^{1/2}$.

the silane alcoholysis reaction to much more polar substrates than previously accessible. We anticipate that with more complex DMA soluble polyol and carbohydrate substrates bearing multiple hydroxyl of more differentiated reactivity, better overall selectivity towards silylations of a single hydroxyl function can be achieved in future studies. Increased yields of selectively silylated products may also be obtainable through the use of excess silane in order to account for reagent loss due to practically unavoidable traces of water in the hygroscopic solvent.

The similarity between the chemical and physical properties of DMF and DMA suggests that **1** would show very similar behaviour in DMA as observed by NMR results in DMF-d_7. Substitution of the labile solvent ligand in **1a** by either the alcohol or the silane, for the latter possibly in an η^2-fashion analogous to the mechanism proposed for $[IrH_2(PPh_3)(THF)_2]SbF_6$ by Luo and Crabtree (8), could start a sequence of reactions leading to the formation of the true catalyst. The composition and structure of the actual active species, however, remain elusive. An NMR scale reaction of **1** with triethylsilane in DMF-d_7 at ambient temperature resulted in complicated ^{1}H and ^{31}P spectra suggesting the formation of at least five different unidentified complexes in solution. Remarkably no signals were observable in the hydride region of the spectrum at this temperature. Upon subsequent addition of an equimolar amount of ethylene glycol to the NMR tube reaction mixture the normal silylation products were again observed.

Conclusion

The new dimeric complex $Ru_2(\mu\text{-}Cl)_2Cl_2(CO)_4(PMe_3)_2$ (**1**) forms an active silane alcoholysis catalyst in DMA. In contrast to the two other homogeneous catalysts systems investigated, $[IrH_2(PPh_3)(THF)_2]SbF_6$ and $RhCl(PPh_3)_3$, **1** does not suffer from coordinative inhibition in this solvent. The heterogeneous system consisting of Pd(0) generated in situ through reduction of PdX_2 (X = Cl$^-$, OAc$^-$) by the silane also is an active catalyst in DMA. The new complex *cis,cis,trans*-$RuCl_2(CO)_2(PMe)_2$ (**3**) isolated from the same reaction mixture as **1** is an active silane alcoholysis catalyst in nonpolar solvents, but completely inactive in DMA.

Experimental

General

All manipulation were performed under a dry argon atmosphere by standard Schlenk-tube techniques. NMR spectra were recorded on a Bruker Avance 400 MHz instrument and IR spectra on a BOMEM FT-IR. ^{1}H NMR spectra simulations were performed using the MEX program (21). For the VT NMR studies the probe temperatures of the NMR spectrometer were independently calibrated using an internal thermocouple. ^{31}P NMR spectra were recorded using a capillary containing 85% H_3PO_4 as the internal standard. GC analyses were performed on a HP 6850 gas chromatograph equipped with a flame ionization detector and integrator.

Mass spectra were obtained with a HP 5970-IN GC-MS spectrometer at the University of Guelph Laboratory Services Division or on a VARIAN Saturn 2000. GC-MS/MS were obtained in our own laboratory. Elemental analyses were performed by Guelph Chemical Laboratories.

Reagents were purchased from Aldrich, Strem Chemicals, Caledon Laboratories, or Fisher Scientific and used as received. Solvents and ethylene glycol were purified by standard techniques and stored under argon. DMA was dried by vacuum distillation from BaO (23) and subsequently stored over activated 4 Å molecular sieves. $[IrH_2(PPh_3)_2(THF)_2]SbF_6$ was synthesized according to the literature methods (8, 14).

Synthesis of $Ru_2(\mu\text{-}Cl)_2Cl_2(CO)_4(PMe_3)_2$ and *cis,cis,trans*-$RuCl_2(CO)_2(PMe_3)_2$

With the exception of the recrystallization procedure, this method is essentially the same as the previously published procedure; carbon monoxide was passed through a boiling solution of ruthenium trichloride dihydrate (0.87 g) in 2-methoxyethanol (25 mL) for 3.5 h. Trimethylphosphine (0.54 g) was added to the hot solution and carbon monoxide was passed through the boiling solution for a further 19 h. The solution had become brownish yellow. The solvent was evaporated under reduced pressure. The resulting greenish-white solid (yield 73%) was recrystallized from CH_2Cl_2–Et_2O giving dimeric species $Ru_2(\mu\text{-}Cl)_2Cl_2(CO)_4(PMe_3)_2Cl_2$ in 38% yield with respect to ruthenium. Subsequent evaporation of the remaining mother liquor and recrystallization of the remaining solid residue from EtOH–water gives the complex *cis,cis,trans*-$RuCl_2(CO)_2(PMe_3)_2$ in 34% yield. Total yield in ruthenium is 34 + 38 = 72%.

*$Ru_2(\mu\text{-}Cl)_2Cl_2(CO)_4(PMe_3)_2$ (**1**)*

For spectroscopic data, see Table 3. Anal. calcd. for $C_{10}H_{18}Cl_4O_4P_2Ru_2$: C 19.74, H 2.98; found: C 19.93, H 3.03.

*$RuCl_2(CO)_2(PMe_3)(O{=}C(CD_3)N(CD_3)_2)$ (**1a**)*

For spectroscopic data see Table 3.

cis,cis,trans-*$RuCl_2(CO)_2(PMe_3)_2$ (**3**)*

For spectroscopic data see Table 3. Anal. calcd. for $C_8H_{18}Cl_2O_2P_2Ru$: C 25.26, H 4.77; found: C 25.48, H 5.21.

X-ray crystal structure determinations

Colourless X-ray quality crystalline samples of both complexes (**1** and **3**) were obtained by slow crystal growth from saturated solutions of the respective solvent–cosolvent mixture at low temperature. Intensity data were collected on a Nonius CAD4 diffractometer. General data collection parameters are listed in Table 5.[6] Accurate cell dimension and crystal orientation matrices were obtained by a least-squares fit of the setting angles of 25 reflections in the ranges indicated in Table 5. Data were acquired using the $\omega - 2\Theta$ method over the ranges indicated in Table 5 and are corrected for Lorentz-polarization and absorption effects. The intensities of 3 standard reflections were measured every 120 reflections and showed 0.8% decay for **1** and no decay for **3**. For both structures the position of the ruthenium atoms were determined by the Patterson method and other nonhydrogen atoms were located by successive difference Fourier syntheses. The structures were refined anisotropically by full-matrix least-squares on F^2. The weighting scheme was $w = 1/[\sigma^2(F_o^2) + (aP)^2 + bP]$ where $P = (F_o^2 + 2F_c^2)/3$. Hydrogen atoms were clearly visible in difference maps and positioned on geometric grounds (C—H 0.96 Å). All calculations were performed using SHELX 97 (24) and PLATON (25) on a Pentium III computer running the LINUX 2.1 operating system.

O-silylation of ethylene glycol

The *O*-silylation reactions of ethylene glycol were conducted by three methods, each of which was found to be most practical depending on the catalyst system used.

Method 1

For catalyst $[IrH_2(PPh_3)_2(THF)_2]SbF_6$; a DMA (3 mL) solution of the Ir catalyst (0.075 mmol = 3 mol% in metal with respect to ethylene glycol) and ethylene glycol (2.5 mmol, 155 mg, 140 μL) was prepared in a three-neck round-bottomed flask fitted with a pressure-equilibrating addition funnel and an Schlenk stopcock. The apparatus was connected to a gas bubbler. A second DMA (3 mL) solution of Et_3SiH (1 eq. = 2.5 mmol, 291 mg, 399 μL or 2 eq. = 5.0 mmol, 582 mg, 798 μL) was prepared in the addition funnel. The silane solution was quickly added with stirring from the addition funnel to the three-neck round-bottomed flask containing the solution of the catalyst and ethylene glycol. The rate of reaction was qualitatively followed by monitoring the speed of the evolved hydrogen with time until hydrogen evolution had stopped indicating the end point of the reaction.

Method 2

For catalysts $RhCl(PPh_3)_3$, $Ru_2(\mu\text{-}Cl)_2Cl_2(CO)_4(PMe_3)_2$, *cis,cis,trans*-$RuCl_2(CO)_2(PMe_3)_2$, and $Co_2(CO)_8$; a DMA, (6 mL) solution of Et_3SiH (1 eq. = 2.5 mmol, 291 mg, 399 μL or 2 eq. = 5.0 mmol, 582 mg, 798 μL) and ethylene glycol (2.5 mmol, 155 mg, 140 μL) was prepared in the addition funnel. The mixed solution was added quickly from the addition funnel to the Schlenk flask containing catalyst (0.075 mmol or 0.0375 mmol for dimer **1** = 3 mol% of metal with respect to ethylene glycol). The rate of reaction was qualitatively followed by monitoring the speed of the evolved hydrogen with time until hydrogen evolution had stopped indicating the end point of the reaction.

Method 3

For catalysts $PdCl_2$ and $Pd(OAc)_2$; a DMA (6 mL) solution of Et_3SiH (1 eq. = 2.5 mmol, 291 mg, 399 μL or 2 eq. = 5.0 mmol, 582 mg, 798 μL) was prepared in an addition fun-

[6] CIF files containing all relevant data for the crystal structure determinations of **1** and **3**, as well as original kinetic data for Fig. 4, have been deposited with CISTI. The supplementary material may be purchased from the Depository of Unpublished Data, Document Delivery, CISTI, National Research Council Canada, Ottawa, ON K1A 0S2, Canada. For information on obtaining material electronically go to http://www.nrc.ca/cisti/irm/unpub_e.shtml. Crystallographic information has also been deposited with the Cambridge Crystallographic Data Centre. Copies of the data can be obtained, free of charge, on application to the Director, CCDC, 12 Union Road, Cambridge CB2 1EZ, U.K. (fax: 44-1223-336033 or e-mail: deposit@ccdc.cam.ac.uk).

nel. The silane solution was added quickly from the addition funnel to a three-neck round-bottomed flask containing the catalyst (0.075 mmol = 3 mol% of metal with respect to ethylene glycol). The system was allowed to equilibrate for 3 min. Ethylene glycol (2.5 mmol, 155 mg, 140 μL) was added via a syringe into the mixture. The rate of reaction was qualitatively followed by monitoring the speed of the evolved hydrogen with time until hydrogen evolution had stopped indicating the end point of the reaction.

Product analysis

The reaction products $Et_3SiOCH_2CH_2OH$, $Et_3SiOCH_2CH_2OSiEt_3$, as well as the side products Et_3SiOH and $Et_3SiOSiEt_3$, were authenticated by ^1H and ^{13}C NMR, and by matching their GC–MS spectra to their known fragmentation patterns available from the NIST compound database supplied with the MS spectrometer software. Quantitative analysis of the reaction mixtures was performed through multi-level calibration of the GC for ethylene glycol, triethylsilane, $Et_3SiOCH_2CH_2OH$, and $Et_3SiOCH_2CH_2OSiEt_3$ over the entire relevant concentration range using authentic compound samples and NMP as an internal standard.

$Et_3SiOCH_2CH_2OH$: ^1H NMR ($CDCl_3$, 298K) δ: 3.65 (m, 4H, $SiOCH_2CH_2OH$), 2.10 (br s, 1H, OH), 0.93 (t, $J_{H,H}$ = 8 Hz, 9H, $Si(CH_2CH_3)_3$), 0.59 (q, $J_{H,H}$ = 8 Hz, 6H, $Si(CH_2CH_3)_3$). ^{13}C NMR ($CDCl_3$, 298K) δ: 63.69, 63.65 (2 s, $SiOCH_2CH_2OH$), 6.67 (s, $Si(CH_2CH_3)_3$), 4.29 (s, $Si(CH_2CH_3)_3$).

$Et_3SiOCH_2CH_2OSiEt_3$: ^1H NMR($CDCl_3$, 298K) δ: 3.64 (s, 4H, $SiOCH_2CH_2OSi$), 0.92 (t, $J_{H,H}$ = 8 Hz, 9H, $Si(CH_2CH_3)_3$), 0.58 (q, $J_{H,H}$ = 8 Hz, 6H, $Si(CH_2CH_3)_3$). ^{13}C NMR ($CDCl_3$, 298K) δ: 64.18 (s, $SiOCH_2CH_2OSi$), 6.37 (s, $Si(CH_2CH_3)_3$), 4.34 (s, $Si(CH_2CH_3)_3$).

Acknowledgments

The authors thank Dr. Alex Bain for help with the MEX simulations and the Natural Sciences and Engineering Research Council of Canada (NSERC), the Canadian Foundation for Innovation (CFI), the Ontario Innovation Trust Fund (OIT), VARIAN Inc., as well as the University of Guelph, for funding.

References

1. M.P. Doyle, K.G. Higgins, V. Bagheri, R.J. Pieters, P.J. Lewis, and M.M Pearson. J. Org. Chem. **55**, 6082 (1990).
2. D.H. Barton and M.J. Kelly. Tetrahedron Lett. **33**, 5041 (1992).
3. T.C. Bedard and J.Y. Corey. J. Organomet. Chem. **428**, 315 (1992).
4. B.T. Gregg and A.R. Cutler. Organometallics, **13**, 1039 (1994).
5. M.J. Burn and R.G. Bergman. J. Organomet. Chem. **472**, 43 (1994).
6. C. Lorenz and U. Schubert. Chem. Ber. **128**, 1267 (1995).
7. S. Chang, E. Scharrer, and M. Brookhart. J. Mol. Catal. A: Chem. **130**, 107 (1998).
8. X.-L. Luo and R.H. Crabtree. J. Am. Chem. Soc. **111**, 2527 (1989).
9. U. Oehmichen and H. Singer. J. Organomet. Chem. **243**, 199 (1983).
10. A.J. Chalk. J. Chem. Soc. Chem. Commun. 847 (1970).
11. I. Ojima, T. Kogure, M. Nihonyanagi, H. Kono, and S. Inaba. Chem. Lett. 501, (1973).
12. R.J. Corriu and J.J.E. Moreau. J. Chem. Soc. Chem. Commun. 38, (1973).
13. R.J.P. Corriu and J.J.E. Moreau. J. Organomet. Chem. **114**, 135, (1976).
14. S.N. Blackburn, R.N. Haszeldien, and R.V. Parish. J. Organomet. Chem. **192**, 329 (1980).
15. L.H. Sommer and J.E. Lyons. J. Am. Chem. Soc. **91**, 7061 (1969).
16. J. M. Blackwell, K.L. Foster, V.H. Beck, and W.E. Piers. J. Org. Chem. **64**, 4887 (1999).
17. H. Singer, E. Hademer, U. Oehmichen, and P. Dixneuf. J. Organomet. Chem. **178**, C13 (1979).
18. C.F.J. Barnard, J.A. Daniels, J. Jeffrey, and R.J. Mawby. J. Chem. Soc. Dalton Trans. 953 (1976).
19. C.K. Johnson. Technical Report ORNL-5138. ORNL, 1976.
20. A.G. Orpen, L. Bramer, F.H. Allen, O. Kennard, D.G. Watson, and R. Taylor. J. Chem. Soc. Dalton Trans. S1 (1989).
21. A.D. Bain and G.J. Duns. J. Magn. Reson. Ser. A, **112**, 258 (1995).
22. R.H. Crabtree, P.C. Demou, D. Eden, J.M. Mihelcic, C.A. Parnell, J.M. Quirk, and G.E. Morris. J. Am. Chem. Soc. **104**, 6994 (1982).
23. M.A. Andrews. Organometallics, **8**, 2703 (1989).
24. G.M. Sheldrick. SHELXL 97. Program for crystal structure determination. Universität Göttingen, Göttingen. 1997.
25. A.L. Spek. PLATON. Program package for crystal structure analysis and display. University of Utrecht, Utrecht. 1999.